R. Rathi[1], P. Gurram[1], S. Mondal[1†], V. Yadav[2], S. Sarkhel[1*], M. V. Sunil Krishna[1], A. K. Upadhayaya[3]

[*]Sumanta Sarkhel, Department of Physics, Indian Institute of Technology Roorkee, Roorkee - 247667, Uttarakhand, India (sarkhel@ph.iitr.ac.in)

[1]Department of Physics,

Indian Institute of Technology Roorkee,

Roorkee - 247667

Uttarakhand, India

[2]Aryabhatta Research Institute of Observational Sciences,

Nainital - 263001

Uttarakhand, India

[3]Environmental Sciences and Biomedical Metrology Division,

CSIR National Physical Laboratory, New Delhi, India

[†]Now at: Physical Research Laboratory,

Ahmedabad - 380009,

Gujarat, India

Abstract

An unusual event of three characteristically different plasma structures on a geomagnetically quiet night (Ap = 4) of 08 July 2018 has been investigated in this paper using an all-sky imager installed at Hanle, Leh Ladakh (32.7°N, 78.9°E; Mlat. ~24.1°N), India. These structures include a freshly generated electrified MSTID (EMSTID), ambiguous plasma depletions, and a northward propagating non-electrified MSTID. One of the most fascinating aspects of this event was the lack of mutual interaction between the three structures, even though they existed simultaneously and propagated in different directions. They individually underwent evolution, distortion, and dissipation separately. One of the structures was an EMSTID, which got generated within the imager's field-of-view (FOV) and evolved with time. As time progressed, different strip-like structures travelled southwestward, merged with each other to form the EMSTID and disappeared later. The second structure was plasma depletions which appeared in the southeastern part of the FOV. They eventually merged into a single band. The merged band evolved with time, extended further northward, and dissipated later. Along with these, a very rare non-electrified MSTID structure with east-west aligned fronts was observed which propagated northward. Its fronts underwent distortion, became curved and dissipated. In this study, we have explored the role of electrodynamics and neutral dynamics behind the observed unique features of the three plasma structures.

Keywords: All-sky imager, O(^{1}D) 630.0 nm airglow, electrified MSTIDs, non-electrified MSTIDs

Key Points:

1. Three characteristically different mutually non-interacting EMSTID, plasma depletion and non-electrified MSTID were observed simultaneously.
2. The EMSTID generated locally and evolved with time, whereas plasma depletions merged into one band.
3. The non-electrified MSTID propagated northward and underwent some distortion, became curved and eventually disappeared.

Plain Language Summary:

Ionospheric plasma irregularities viz. traveling ionospheric disturbances (TIDs), plasma bubbles, spread F have been studied using different techniques such as airglow, radar, ionosonde, GPS-TEC, etc. On the night of 08 July 2018, we observed a rare event consisting of three different plasma irregularities/structures simultaneously over Hanle, Leh Ladakh, India in the 630.0 nm airglow images. The three structures were freshly generated electrified MSTID (EMSTID), ambiguous plasma depletions, and non-electrified MSTID. All the three plasma structures exhibited different characteristics. One of the interesting aspects of the event was non-interaction between these three structures despite existing simultaneously. They underwent evolution, distortion, and dissipation separately. EMSTID evolved within the imager's FOV and later dissipated, whereas the plasma depletions merged with each other, became more prominent, and dissipated in the end. Other structure was the east-west (EW) oriented northward propagating non-electrified MSTID, which later became curved and dissipated in the end. In this study, we explored the plausible reasons for the observed rare features using multi-instrument and model-based data.

1. Introduction

The Earth's ionosphere exhibits different kind of plasma irregularities, which have potential impact on the satellite-based communication and navigation systems. Traveling ionospheric disturbances (TIDs) are wave-like plasma density disturbances having a variety of scale sizes that propagate in the ionospheric F-region. Initially, they were believed to be caused by the perturbation of ionized layer modulated by gravity waves (Hines, 1960). TIDs are classified into two categories depending upon their scale sizes. These are medium scale TIDs (MSTIDs) and large scale TIDs (LSTIDs). MSTIDs are the most persistent and prominent in the mid-latitude ionosphere. For the past few decades, various techniques have been used to study MSTIDs such as ionosondes, satellite beacons, ground-based Global Navigation Satellite System (GNSS) networks, HF Doppler radars and airglow imagers (Amorim et al., 2011; Garcia et al. 2000; Huang et al., 2018, 2016; Hunsucker, 1982; Shiokawa, Ihara et al., 2003;

Shiokawa, Otsuka et al., 2003; and references therein). MSTIDs are propagating low and high plasma density wavefronts, which appear as propagating dark and bright bands in 630.0 nm airglow images (Shiokawa, Ihara et al., 2003; Shiokawa, Otsuka et al., 2003). They propagate with phase speed of 50-150 m/s and have wavelength in the range of 100-500 km (Duly et al., 2013; Garcia et al., 2000; Narayanan et al., 2014; Pimenta et al., 2008). They are broadly classified into two types depending on the generation mechanism (i) electrified MSTIDs (ii) non-electrified MSTIDs (Figueiredo et al., 2018; Narayanan et al., 2019; Otsuka et al., 2013; Paulino et al., 2018, 2016; Pimenta et al., 2008). The electrified MSTIDs (EMSTIDs) are associated with polarization electric field and have preferential direction of propagation (Perkins, 1973; Shiokawa, Ihara et al., 2003). The phase fronts of EMSTIDs in the northern (southern) hemisphere align predominantly in northwest-southeast (northeast–southwest) direction and propagate southwestward (northwestward) during nighttime (Ding et al., 2011; Huang et al., 2018, 2016; Otsuka et al., 2004; Shiokawa et al., 2005; Shiokawa, Ihara et al., 2003; Sun et al., 2015). EMSTIDs originate through Perkins' instability (Perkins, 1973), which successfully explains the orientation of nighttime EMSTIDs. By using numerical simulations, Zhou et al. (2006) validated the Perkins' explanation. However, since the Perkins' instability's growth rate is too low, it requires additional seeding processes to generate EMSTIDs (Behnke, 1979; Garcia et al., 2000; Kelley & Fukao 1991; Kelley & Makela, 2001; Perkins, 1973; Otsuka et al., 2004; Otsuka et al., 2007; Shiokawa et al., 2005). The seeding processes include gravity waves, E-F coupling, and/or interhemispheric coupling. Gravity waves traveling from lower atmosphere to thermosphere can generate undulations. Perkins' instability can amplify these undulations and generate EMSTIDs (Huang et al., 1994; Kelley & Fukao, 1991). Further, Cosgrove and Tsunoda (2004) have suggested that sporadic E (Es) layers can provide seeding for the nighttime EMSTIDs. Yokoyama et al. (2009) simulated the formation of MSTID's frontal structures via sporadic E layer coupling process. These seeding processes can play a vital role in accelerating the Perkins' instability growth rate by providing polarization electric field in the F region. The polarization electric field associated with MSTIDs generates undulation in the base height (h'F) of the ionosphere (Amorim et al., 2011; Rathi et al., 2021; Shiokawa, Ihara et al., 2003).

Although MSTIDs generally propagate equatorward irrespective of the hemisphere, there are a few studies, which have reported poleward propagating MSTIDs. These are manifestation of gravity waves in the F region and known as gravity wave MSTIDs or non-electrified MSTIDs. The gravity wave MSTIDs can have any orientation and propagation direction based on the wave source (Figueiredo et al., 2018; Paulino et al., 2018, 2016). The SuperDARN Hokkaido radar observed a few cases of MSTIDs having northward propagation (Ichihara et al., 2013). In a statistical study, Shiokawa et al. (2013) also reported northward moving MSTIDs from Athabasca. A thermospheric wave signature propagating northward has been reported by Sau et al. (2018) from the Indian sector.

More attention has been given in recent years to interaction of an MSTID with other plasma structures. Otsuka et al. (2012) reported encounter of a MSTID with an equatorial plasma bubble, which resulted in dissipation of the bubble. Of late, Yadav, Rathi, Sarkhel et al. (2021) and Yadav, Rathi, Gaur et al. (2021) reported complex interactions between MSTIDs and field aligned plasma depleted structures from Hanle, India which is a transition region of geomagnetic low-mid latitudes. From the same location Rathi et al. (2022) recently reported an interaction between two fronts of a MSTID followed by bifurcation and dissipation of the fronts. Along with the MSTIDs' interaction, a number of interesting events have also been observed over the Hanle region over the last few years. Sivakandan et al. (2020, 2021) reported rare cases of mid-latitude spread F (MSF) and in situ generated plasma bubble over the Hanle region. In another study, Rathi et al. (2021) reported simultaneous occurrence of the single dark band and periodic MSTIDs. Though characterization of MSTIDs has been done numerous times previously, there are still limited studies on the interaction of MSTIDs with other plasma structures.

This paper presents a unique observation of simultaneously existing three different plasma structures over the Hanle region. It is interesting to note that despite existing simultaneously these structures did not appear to interact mutually, rather individually underwent transformations. We have investigated the role of electrodynamics and neutral dynamics behind the observed features of the three plasma structures.

2. Instruments and Data Analyses

We have used the 630.0 nm airglow data from the night of 08 July 2018 from a multi-wavelength all-sky airglow imager installed at Hanle, Leh Ladakh, India (32.7°N, 78.9°E; Mlat. ~24.1°; Height: ~4200 m above mean sea level) which lies at the transition of geomagnetic low and mid-latitudes. All the details of the imager and image processing are available in Mondal et al. (2019). In order to complement the airglow imager data, we have used the 15 min resolution ionograms obtained from New Delhi digisonde (28.70°N, 77.10°E; Mlat. ~20.2°N). Therefore, the digisonde is useful for studying the ionospheric irregularities and background conditions along with the Hanle airglow imager as the observation regions of the two instruments share a partially common volume. We scaled the F layer base height (h'F) manually and examined the occurrence of spread F and sporadic E layer by using the ionograms. A more detailed description of the digisonde is available in Upadhayaya and Mahajan (2013).

3. Results

A unique event of three characteristically different plasma structures was observed on 08 July 2018 in the O(^{1}D) 630.0 nm airglow images over Hanle, Leh Ladakh, India. These structures were recorded on a geomagnetically quiet night which lies in low solar flux period (Ap = 4, F10.7 = 74). Figures 1 & 2 show the existence of three plasma structures having different characteristics, which started appearing in the imager's FOV from 16:08:24 UT or 21:38:24 IST (In-

dian Standard Time (IST) = UT + 5.5 h) and continued to stay until 20:06:37 UT (01:36:37 IST, 09 July 2018). Here, the most striking features were the contrasting behaviors of the three observed structures and the apparent lack of any mutual interaction between them, even though they existed simultaneously. The detailed descriptions on these structures and their features are described below.

3.1 Non-interacting three different plasma structures

Out of the above mentioned three distinct plasma structures, the two plasma structures are clearly visible in Figure 1. It shows the sequence of the 630.0 nm unwarped images in which the red stars and red triangles represent the location of Hanle imager and New Delhi digisonde respectively. The vertical red dashed-dotted line represents the direction of geomagnetic north-south (NS) over Hanle. The first structure, consisting of multiple northwest-southeast (NW-SE) aligned fronts propagating in the southwest (SW) direction, was observed in the central part of the images from 16:08:24 UT (21:38:24 IST) to 18:57:40 UT (00:27:40 IST, 09 July 2018). Initially these multiple fronts were very thin and faint strip-like structures (Figures 1a-c). As time progressed, these fainter strips started merging with each other, evolved into two prominent groups of bands (Figure 1e) and propagated further. Finally, these bands became defused and disappeared within the imager's FOV.

The second type of structure is a couple of plasma depleted fronts observed close to the southeastern edge of the images between 17:23:28 UT (22:53:28 IST) and 17:54:59 UT (23:24:59 IST). These are marked with cyan dotted lines and named as 'd_1' and 'd_2' (Figures 1f-h). Since only a small part of them was visible within the FOV, we were unable to distinguish whether they were a part of MSTIDs or a manifestation of plasma bubbles. Hence, we are calling them just as plasma depleted fronts. These fronts ('d_1' and 'd_2') evolved with time and later between 17:54:59 UT (23:24:59 IST) and 18:07:31 UT (23:37:31 IST) merged with each other forming a single band named as 'D'. As time progressed this band 'D' became much more conspicuous and extended further northward within the FOV (Figures 1i-k). Later, it started decaying nearly from 18:45:08 UT (00:15:08 IST, 09 July 2018) and almost disappeared within the FOV (Figures 1l-o). It is worth noting that these two structures, one at central part and other at southeastern edge, did not interact with each other even though they existed simultaneously. For the reader's convenience, the complete sequence of images on that night is reproduced in the form of a movie which is available in the supplementary material of this paper.

Apart from the two types of structures described above, another plasma structure with very faint alternate high and low intensity bands was also observed from the beginning. Since these bands were very faint, it was very challenging to identify them in the unwarped images. In order to improve their visibility and identify their features clearly, we have presented successive difference images in Figure 2. It shows a sequence of these images, showing northward propagating alternate bright and dark bands from 16:14:40 UT (21:44:40 IST) to 17:48:43

UT (23:18:43 IST). The yellow arrow in Figure 2a indicates the alternate bright and dark bands, which were oriented in the east-west (EW) direction and were propagating northward. The horizontal velocity and wavelength of these bands were found to be 113 ± 15 m/s and 175 ± 21 km, respectively. Initially, these northward propagating bands appeared to as plane wavefronts (Figures 2a-b) and as time progressed these plane wavefronts distorted, became curved, and eventually dissipated (Figures 2c-o). For the reader's convenience, the sequence of successive difference images on that night is reproduced in the form of a movie which is available in the supplementary material of this paper.

Within a period of nearly four hours, we simultaneously observed these three structures having different characteristics. The most intriguing aspect of this event was that despite existing simultaneously, the structures didn't seem to interact with each other.

3.2 Ionosonde Observations from New Delhi

In order to investigate background conditions and effects of the observed structures, we have utilized ionograms from a nearby digisonde at New Delhi, which is marked by red triangles in Figures 1 & 2. A sequence of few ionograms is prepared and shown in Figure 3. We observed a clear rise and fall in the F layer trace and few ionograms showed presence of spread F. Furthermore, we manually scaled the ionograms to get the F layer base height (h'F) and the variation of the h'F with time is shown in Figure 4. Red asterisks and blue diamond are showing the presence of spread F and blanketing sporadic E (Esb) layer respectively. Black vertical dashed lines represent the start and end time of the airglow observations on that night. between 14 UT (19.50 IST) and 16.50 UT (22 IST), h'F decreased gradually and after that, it increased till 17.25 UT (22.75 IST), followed by another decrease in the h'F up to 18.30 UT (23.80 IST). Beyond this, a sharp upliftment of the F layer was observed reaching nearly 300 km at around 20 UT (01.50 IST, 09 July 2018).

3.3 Neutral wind on 08 July 2018

In order to explain the generation, morphology and different features of the observed structures, we examined the role of nighttime neutral winds. Since actual observations of neutral wind are not available, we looked at the neutral wind values obtained from the horizonal wind model (HWM14) (Drob et al., 2015). We obtained the horizontal and meridional wind velocity in the same region covered by the all-sky imager. Figure 5 shows the variation of meridional wind between 15:20 UT (20:50 IST) and 20 UT (01:30 IST, 09 July 2018). The horizontal wind velocity is plotted between 16:15 UT (21:45 IST) and 18:45 UT (00:15 IST, 09 July 2018) in Figure 6. Blue arrows represent the direction of the horizontal wind, and it was southeastward during this period with higher southward (equatorward) component. These two figures show that the wind was equatorward and its magnitude increased with time during the event.

4. Discussion

Three characteristically different plasma structures were observed simultaneously over the Hanle on 08 July 2018. This day was geomagnetically quiet (Ap = 4) and falls in low solar flux period (F10.7 = 74), which discarded any role of geomagnetic disturbances (storm and sub-storm). We investigated this event using data from multiple instruments and model. Section 3 covers all the unique results of this event. The possible mechanisms behind the observed structures and their features have been discussed hereafter.

4.1 Freshly generated electrified MSTID (EMSTID)

MSTIDs generated through Perkins' instability are also known as electrified MSTIDs (EMSTIDs), as these structures are accompanied by large electric fields (Crowley & Rodrigues, 2012). They propagate in preferential direction towards SW (NW) with NW-SE (NE-SW) oriented fronts in the northern (southern) hemisphere. Different studies provided good insights in understanding EMSTIDs during various seasons and solar cycle (Narayanan et al., 2014; Pimenta et al., 2008). In the East Asian sectors, EMSTIDs occur primarily during solstices with primary maxima during June solstices. In the present event, on a geomagnetically quiet night during June solstice, we observed very faint NW-SE aligned thin strip-like structures in the center of the airglow images, which started appearing nearly from 16:08 UT (shown in Figure 1). As time progressed, these thin strips became prominent and appeared to interact with each other while propagating in the SW direction. This gives the impression that the strips were merging with each other to evolve into two separate groups. The two groups appeared as two NW-SE aligned dark bands, which propagated towards SW (Figures 1f-j). The observed thin strips appeared in the center of the images, rather than propagating somewhere from NE of Hanle. The above results imply that they might be freshly or locally generated EMSTID over Hanle region. Yadav, Rathi, Gaur et al. (2021) have reported one such case of locally generated Perkins' MSTID or EMSTID from the same imager on 06 May 2019. These results indicate that EMSTIDs can even generate over the geomagnetic low-mid latitude transition regions.

Though EMSTIDs are generated through Perkins' instability mechanism, it alone may not be very efficient in producing EMSTIDs due to its low growth rate (Garcia, 2000; Kelley & Fukao, 1991; and references therein). This necessitates some sort of seeding mechanism, such as gravity waves, ionospheric E-F coupling, and inter-hemispheric coupling (Behnke, 1979; Cosgrove et al., 2004; Cosgrove & Tsunoda, 2004; Fukao et al., 1991; Huang et al., 1994; Kelley et al., 2000; Kelley & Fukao, 1991; Otsuka et al., 2004; Otsuka et al., 2007; Shiokawa et al., 2005; Tsunoda & Cosgrove, 2001). For the present case of locally generated EMSTIDs over Hanle, we looked for a possible source of seeding for their generation. Gravity waves generated in the lower atmosphere can seed the Perkins' instability in the ionospheric F region and help in generation of EMSTIDs (Huang et al., 1994; Kelley & Fukao, 1991). In order to check any role of atmospheric gravity waves, we looked into the O(^{1}S) 557.7 nm airglow images from Hanle. These images did not show any gravity waves, which discarded the

role of the lower atmospheric gravity waves in the observed EMSTID's generation. However, it might be possible that thermospheric gravity waves generated at the bottom of the F region aided the generation of the observed EMSTID. In addition to the gravity waves, sporadic E (Es) layers may join the Perkins' instabilities by coupling between the ionospheric E and F region (Cosgrove & Tsunoda, 2004; Kelley et al., 2003; Tsunoda & Cosgrove, 2001;). Researchers previously demonstrated that the Hall polarization electric fields generated in the E layer instabilities interact with the polarization electric fields generated by the Perkins' mechanism in the F region (Tsunoda & Cosgrove, 2001). Otsuka et al. (2007) and Ogawa et al. (2009) identified simultaneous occurrences of MSTIDs and Es. It is important to note that E and F regions are coupled with regions within a hemisphere as well as to the regions from the other hemisphere. Otsuka et al. (2004) and Shiokawa et al. (2005) had previously reported conjugated MSTIDs from the Japanese and Australian longitudinal sector. There is also a possibility that the observed MSTIDs were caused by polarization electric fields provided through interhemispheric coupling from the conjugated hemisphere. Since we didn't have any observations from the conjugate point, we are unable to comment on the interhemispheric coupling. The above-mentioned seeding mechanisms increase the growth rate, leading to the generation of irregularities within a reasonable time (Yokoyama et al., 2009; Yokoyama, 2013, 2014; Yokoyama & Hysell, 2010). The seeding theories seem to be validated by experimental observations (Chen et al., 1972; Otsuka et al., 2008, 2007; Saito et al., 2007). In their simulation, Yokoyama et al. (2009) demonstrated that coupling between E and F layer can dramatically increase the Perkins' instability growth rate as well as predict the formation of a westward propagating NW-SE aligned MSTID fronts. Based on a simulation study, Yokoyama (2013) generated such wave fronts, in which the author investigated the coupled dependence of the Es layer instability and the frontal formation of MSTIDs on the wavelength of the initial perturbations. The present case appears similar to the frontal formation in Yokoyama (2013), where the initial fronts were very thin and had irregular shapes. As time progressed, these fronts evolved and merged with each other and eventually formed NW-SE aligned EMSTIDs' fronts. It might be possible that the Es layers somewhere northward of Hanle seeded the Perkins' instability and helped in generation of the observed EMSTID over Hanle. Unfortunately, we didn't have any data from the north of Hanle. Therefore, the role of E-F coupling cannot be examined here. Previous studies and present results indicate that the observed EMSTID was probably generated through E-F coupling or interhemispheric coupling.

4.2 Ambiguous plasma depleted fronts

We observed two plasma depleted fronts 'd_1' and 'd_2' close to southeastern edge of the imager's FOV (Figures 1f-h) from 17:23:28 UT (22:53:28 IST). As time progressed, these bands propagated in the FOV and later they got merged into a single depletion 'D' (Figure 1i). Since the plasma depleted fronts 'd_1', 'd_2' and the merged band 'D' had only a small portion in the FOV close to the southeastern edge and were evolving with time, we were unable to ascertain

whether they were the part of an MSTID or Plasma bubble. Thus, they were named as ambiguous plasma depleted fronts. The merged structure 'D' evolved with time, became much more prominent and extended up to further northern latitudes (Figures 1i-k). Initially, the northern extent of the merged plasma depletion 'D' was up to 31.35°N latitude denoted as P_1 (Figure 1i), later it extended up to 33.4°N latitude denoted as P_2 (Figure 1k). The extension of the observed plasma depletion 'D' might be due to mutual interaction between 'd_1' and 'd_2' and/or due to the equatorward neutral winds.

Any plasma structure in northern hemisphere can extend further northward when it reaches a higher altitude, at that point it follows the geomagnetic field lines and mapped to higher latitudes. In mid-latitudes, the increment/decrement in the height of the ionospheric F layer is connected to meridional winds and/or zonal electric fields (Amorim et al., 2011; Joshi et al., 2016; Rout et al., 2018; Shiokawa et al., 2015; Sun et al., 2019). In the northern hemispheric mid-latitude regions, equatorward wind causes an increase in the h'F, while poleward wind decreases h'F (Rishbeth et al., 1987). Particularly in low-mid latitude region where the electric fields have less effect than at equatorial latitudes, polarity of the wind plays an important role in determining the height of the F layer. During quiet time summer months, the nighttime meridional wind flows equatorward (Fejer et al., 2002; Kawamura et al., 2000). As a part of the study, we also investigated the role of the meridional winds over Hanle region using horizonal wind model (HWM14) (Drob et al., 2015). We analyzed the meridional winds for ±5° latitude-longitude regions around Hanle from 15:20 to 20 UT and observed the presence of stronger equatorward wind (Figure 5). The direction of the modeled wind matches well with the previously observed winds during summer; however, the magnitude may differ from actual observations. There was a stronger equatorward wind nearly from 18:20 UT (Figures 5j-o), along with it we observed a clear rise in the h'F nearly from 18.5 UT (Figure 4). In addition, during this time no plasma structure passed over the New Delhi digisonde. The equatorward wind might have pushed the ionized layer from higher latitude to lower latitude and raised the F-layer to higher altitudes over low-mid latitude regions. Generally, the ambient electric field controls the F-region altitude through $\mathbf{E} \times \mathbf{B}$ drifts. Eastward electric field causes an upward $\mathbf{E} \times \mathbf{B}$ drift and hence F layer height increases. Assuming the plasma depletions 'd_1' and 'd_2' had eastward component of electric field, when they interacted with each other, the two eastward electric fields superimposed and formed a stronger resultant electric field ($\mathbf{E}_\mathrm{R}$). This resultant electric field ($\mathbf{E}_\mathrm{R}$) with the geomagnetic field ($\mathbf{B}$) caused a higher upward $\mathbf{E}_\mathrm{R} \times \mathbf{B}$ drift. Due to which the merged plasma front 'D' attained higher altitude and mapped to higher latitude regions through mapping along the geomagnetic field lines. Both the equatorward wind and the resultant electric field ($\mathbf{E}_\mathrm{R}$) played the role in the northward extension of the merged plasma depletion 'D'.

4.3 Northward propagating non-electrified MSTID

In the mid latitudes, the nighttime MSTIDs, generated by the Perkins' instability, usually propagate towards SW with NW-SE aligned phase fronts (Perkins, 1973). Previous reports from Hanle imaging observations give the weightage on the predominant NW-SE aligned Perkins' MSTIDs (Rathi et al., 2021; Rathi et al., 2022; Yadav, Rathi, Gaur et al., 2021; Yadav, Rathi, Sarkhel, et al., 2021). However, on the night of 08 July 2018, we observed EW aligned northward propagating wave, somehow different from the EMSTIDs. Very few studies have reported similar northward propagating wave structures and their detailed characteristics. Ichihara et al. (2013) observed northward propagating MSTIDs and concluded that upward propagating gravity waves were responsible for such unusual poleward propagation. Bhat et al. (2021) observed EW aligned northward moving MSTIDs over the low-mid latitude region (Srinagar, India) in the northern hemisphere. They suggested that the atmospheric gravity waves travelling from lower atmosphere were responsible for the northward propagating MSTIDs in the northern hemisphere. According to Hines (1960), if gravity waves were to blame for the observed northward moving structures, they would follow a linear dispersion relation i.e,

$$m^2 = \frac{N^2}{(u-c)^2} - k^2 - \frac{1}{4H^2}$$

Here, m $(2\,/\,{}_z)$ is the vertical wave number, where ${}_z$ is vertical wavelength, N is the Brunt Vaisala frequency, g is the acceleration due to gravity and H is the scale height, u is the background wind velocity projected along the wave vector, and c is apparent wave phase velocity, k $(2\,/\,{}_h)$ is the horizontal wave number, where ${}_h$ is the horizontal wavelength. In order to get estimate of the scale height at the Hanle region, we used the MSISE00 model (Hedin et al., 1991). At 250 km, the scale height was 20 km. At 250 km, projected wind (u) was derived from horizontal wind model for this night. Taking ${}_h = 175$ km and $c = 113$ m/s as typical values and projected wind, $u = 40$ m/s, the vertical wavelength ${}_z$ would be nearly 112 km. For the gravity wave activity to be observed in an emission layer, the vertical wavelength (${}_z$) of the gravity wave must be greater than the layer thickness. This is consistent with our results, since the vertical wavelength of the gravity waves observed in the 630.0 nm airglow images was larger than the emission thickness of ~80 km (Sobral et al., 1993). A ray tracing study by Vadas (2007) determined gravity wave propagation characteristics and dissipation altitudes. It was found that gravity waves require horizontal wavelengths greater than 100 km to reach height more than 200 km (refer to Figure 9b in Vadas, 2007). The horizontal wavelength (${}_h$) of the observed bands was 175 ± 21 km. Furthermore, the authors have shown that if the gravity waves are reaching above 200 km, it must have a minimum intrinsic phase speed of 100 m/s. In the present case the intrinsic phase velocity was 153 ± 15 m/s. All these results imply that the gravity wave might have reached above 200 km and appeared in the 630.0 nm airglow images as gravity wave MSTID.

The gravity waves propagating from the lower atmosphere are subject to damping by kinematic viscosity, thermal diffusivity, and critical level filtering (Fritts and Vadas, 2008; Vadas, 2007; Vadas and Fritts, 2005). The gravity wave damping via viscous dissipation and thermal diffusion depends on its vertical wavelength, intrinsic frequency, and phase speed (Vadas, 2007; Vadas and Fritts, 2005). However, the gravity waves with larger wavelength ($_z$) are less vulnerable to the dissipative filtering (via viscous dissipation and thermal diffusion). If the gravity waves have smaller $_z$, it enhances the effects of dissipative filtering, thereby accelerating the gravity waves' dissipation (Vadas, 2007). Whereas, the critical level filtering damps the gravity waves by middle atmospheric neutral winds (Fritts and Vadas, 2008). However, this process preserves the gravity waves traveling oppositely to the neutral wind. In the present scenario, the estimated mean wind speed (u) was ~40 m/s, opposite to the wave propagation direction (Figure 6). As the velocity of the northward propagating waves differed from the background wind velocity and direction, the observed wave was not subject to critical level filtering and thus propagated to the thermospheric heights. Shiokawa et al. (2006) had earlier observed similar type of EW oriented quasi-periodic southward moving waves and suggested their generation through gravity waves and not by the thermospheric oscillating electric field. Any kind of east/west directed polarization electric field, is unable to generate the observed EW oriented fronts. Overall, the northward propagating MSTIDs (EW alignment) are generated by gravity waves, and called as non-electrified MSTIDs or gravity wave MSTIDs. However, gravity waves can be generated at any latitude and longitude and can have any propagation direction. They can originate in the lower (troposphere, stratosphere, mesosphere) as well as in upper atmosphere (thermosphere) (Yiğit et al., 2020). Hocke et al. (1996) and Nicolls et al. (2014) suggested ion drag by gravity waves causes neutral oscillations in the F region, thus producing non-electrified or gravity wave MSTID. In order to verify whether locally generated gravity waves played any role in the observed northward propagating MSTID, we examined the 557.7 nm airglow images on the same night over Hanle region. It revealed that there was no signature of locally generated gravity wave activity. Therefore, any locally generated gravity waves were not involved in the generation of the MSTID. However, involvement of non-native gravity wave in generating northward moving observed MSTID is plausible.

In addition to the northward propagation, the gravity wave MSTID exhibited another interesting feature. Initially, the wavefronts were observed as plane wavefronts (Figures 2a-b). As time progressed, the plane fronts became curved and dissipated later (Figures 2c-o). In order to find out the possible reason behind the transformation of the fronts, we looked into the neutral winds over Hanle. Since we did not have any direct observation of neutral winds over Hanle, we checked the HWM14 wind values. Figure 5 shows the variation of the meridional wind velocity at 250 km on the night of 08 July 2018 obtained using HWM14. The meridional winds were equatorward during the event time and its magnitude increased with time. Along with the increment in the magnitude,

there was a zonal gradient in the meridional wind between 16:20 UT and 17:40 UT (Figures 5d-h). The equatorward wind speed was lower in the western part and increased towards east, indicating a zonal gradient. As the plane wavefronts of the gravity wave MSTID experienced this gradient, the eastern part of the plane wavefronts started bending and later fronts became curved.

4.4 A trio of non-interacting plasma structures

The observed three plasma structures existed simultaneously and underwent evolution, deformation, and dissipation separately. We have discussed these features of each individual structure in the previous sections. Here the main question arises, why these structures did not interact with each other, even though they existed simultaneously. There are previous studies, which reported interaction between simultaneously existing different ionospheric plasma structures viz. MSTIDs, plasma depletions (Otsuka et al., 2012; Rathi et al., 2022; Yadav, Rathi, Gaur et al., 2021; Yadav, Rathi, Sarkhel et al., 2021). In these studies, authors explained the electrostatic interactions through the polarization electric fields associated with these structures. In the present case, the observed three structures appeared to be non-interacting. The first two structures, EMSTID and ambiguous plasma depletions did not interact mutually, possibly because they were quite separated from each other (Figures 1f-k). The most intriguing aspect of this event was the lack of interaction between southwestward propagating EMSTID and northward propagating non-electrified MSTID, even though they traversed the same region simultaneously (Figures 1 & 2). The absence of any polarization electric field within the non-electrified MSTID could be a reason for their lack of interaction. However, such 'non-interactions' between overlapping electrified and non-electrified plasma structures need further investigations to provide more insights.

5. Summary and Conclusions

Using multi-instrument (630.0 nm airglow imager and digisonde) and model simulated data, we investigated a unique event that occurred on the night of 08 July 2018 over geomagnetically transition region of low-mid latitude. Here, we simultaneously observed three characteristically different plasma structures over the Hanle region. The main conclusions of this study are as follows:

1. The first plasma structure was the locally generated electrified MSTID, which evolved with time and propagated southwestward. As time progressed, different fronts of the EMSTID merged with each other, became more prominent, and eventually dissipated. The E-F coupling might be the probable cause for the generation of EMSTID over the Hanle region.

2. In addition, we observed two ambiguous plasma depleted fronts, which later merged with each other and formed a single band. This merged single band evolved with time, became more prominent, and extended further northward. This northward extension of the merged front was caused combinedly by the stronger equatorward wind and the resultant eastward electric field.

3. An unusual northward propagating non-electrified MSTID (gravity wave MSTID) was also observed. Initially, the wavefronts of the MSTID were plane fronts with EW alignment. Over time, the plane fronts of this MSTID became curved, possibly due to a gradient in the meridional wind in longitudinal directions.

4. Despite existing simultaneously, these structures did not interact mutually, rather they individually underwent their own evolution, distortion, and dissipation.

Data Availability Statement

The data sets utilized in this study are available at https://doi.org/10.5281/zenodo.6508537. The neutral wind data was obtained from Horizontal Wind Model (HWM14). Geomagnetic activity indices were obtained from WDC, Kyoto (https://wdc.kugi.kyoto-u.ac.jp/kp/index.html#LIST). Solar flux index (F10.7) is obtained from CDAWeb (https://cdaweb.gsfc.nasa.gov/index.html). MSISE00 model data is available at https://ccmc.gsfc.nasa.gov/modelweb/models/nrlmsise00.php.

Acknowledgments

S. Sarkhel acknowledges the financial support from the Science and Engineering Research Board, Department of Science and Technology, Government of India (EMR/2016/000247) to procure the multi-wavelength airglow imager. The support from Indian Astronomical Observatory (operated by Indian Institute of Astrophysics, Bengaluru, India), Hanle, Leh Ladakh, India for the day-to-day operation of the imager is duly acknowledged. R. Rathi acknowledges the fellowship from the Innovation in Science Pursuit for Inspired Research (INSPIRE) programme, Department of Science and Technology, Government of India. P. Gurram acknowledges the fellowship from Indian Institute of Technology Roorkee. S. Mondal acknowledges the fellowship from the Ministry of Education, Government of India for carrying out this research work. This work is also supported by the Ministry of Education, Government of India.

References

Amorim, D. C. M., Pimenta, A. A., Bittencourt, J. A., & Fagundes, P. R. (2011). Long-term study of medium-scale traveling ionospheric disturbances using OI 630 nm all-sky imaging and ionosonde over Brazilian low latitudes. *Journal of Geophysical Research: Space Physics, 116*(6), 1–7. https://doi.org/10.1029/2010JA016090.

Behnke, R. (1979). F layer height bands in the nocturnal ionosphere over Arecibo. *Journal of Geophysical Research, 84(A3),* 974–978. https://doi.org/10.1029/JA084iA03p00974.

Bhat, A. H., Ganaie, B. A., Ramkumar, T. K., & Malik, M. A. (2021). Northward propagation of medium scale traveling ionospheric disturbances over Srinagar, J and K India. *Advances in Space Research, 68(9),* 3806–3813. https://doi.org/10.1016/j.asr.2021.06.035.

Chen, A. A., Chin, P. N., & Chance, M. P. (1972). Field-line connection between scintillation and ionospheric conditions causing spread E. *Journal of Geophysical Research, 77(10),* 1859–1868. https://doi.org/10.1029/JA077i010p01859.

Cosgrove, R. B., & Tsunoda, R. T. (2004). Instability of the E-F coupled nighttime midlatitude ionosphere. *Journal of Geophysical Research, 109,* A04305. https://doi.org/10.1029/2003JA010243.

Cosgrove, R.B., Tsunoda, R.T., Fukao, S., Yamamoto, M. (2004). Coupling of the Perkins instability and the sporadic e layer instability derived from physical arguments. *Journal of Geophysical Research,* 109, A06301. https://doi.org/10.1029/2003JA010295.

Crowley, G., & Rodrigues, F. S. (2012). Characteristics of traveling ionospheric disturbances observed by the TIDDBIT sounder. *Radio Science, 47(4).* https://doi.org/10.1029/2011rs004959.

Ding, F., Wan, W., Xu, G., Yu, T., Yang, G., & Wang, J. (2011). Climatology of medium-scale traveling ionospheric disturbances observed by a GPS network in central China. *Journal of Geophysical Research: Space Physics, 116*(A9), n/a–n/a. https://doi.org/10.1029/2011ja016545.

Drob, D. P., Emmert, J. T., Meriwether, J. W., Makela, J. J., Doornbos, E., Conde, M., Klenzing, J. H. (2015). An update to the Horizontal Wind Model (HWM): the quiet time thermosphere. *Earth and Space Science, 2(7),* 301–319. https://doi.org/10.1002/2014ea000089.

Duly, T. M., Chapagain, N. P., & Makela, J. J. (2013). Climatology of nighttime medium-scale traveling ionospheric disturbances (MSTIDs) in the Central Pacific and South American sectors. *Annales de Geophysique, 31(12),* 2229–2237. https://doi.org/10.5194/angeo-31-2229-2013.

Fejer, B. G., Emmert, J. T., & Sipler, D. P. (2002). Climatology and storm time dependence of nighttime thermospheric neutral winds over Millstone Hill. *Journal of Geophysical Research, 107(A5).* https://doi.org/10.1029/2001ja000300.

Figueiredo, C. A. O. B., Takahashi, H., Wrasse, C. M., Otsuka, Y., Shiokawa, K., & Barros, D. (2018). Investigation of nighttime MSTIDs observed by optical thermosphere imagers at low latitudes: Morphology, propagation direction, and wind filtering. *Journal of Geophysical Research: Space Physics, 123*, 7843–7857. https://doi.org/10.1029/2018ja025438.

Fritts, D. C., & Vadas, S. L. (2008). Gravity wave penetration into the thermosphere: sensitivity to solar cycle variations and mean winds. *Annales Geophysicae, 26(12),* 3841–3861. https://doi.org/10.5194/angeo-26-3841-2008.

Fukao, S., Kelley, M. C., Shirakawa, T., Takami, T., Yamamoto, M., Tsuda, T., & Kato, S. (1991). Turbulent upwelling of the mid-latitude ionosphere: 1. Observational results by the MU radar. *Journal of Geophysical Research, 96(A3),* 3725. https://doi.org/10.1029/90ja02253.

Garcia, F. J., Kelley, M. C., Makela, J. J., & Huang, C.-S. (2000). Airglow observations of mesoscale low-velocity traveling ionospheric disturbances at midlatitudes. *Journal of Geophysical Research: Space Physics, 105(A8),* 18407–18415. https://doi.org/10.1029/1999ja000305.

Hines, C. O. (1960). Internal atmospheric gravity waves at ionospheric heights. Canadian Journal of Physics, 38 (11), 1441-1481. https:// doi.org/10.1139/p60-150.

Hedin, A. E. (1991). Extension of the MSIS Thermosphere Model into the middle and lower atmosphere. *Journal of Geophysical Research: Space Physics, 96(A2),* 1159–1172. https://doi.org/10.1029/90ja02125.

Hocke, K. & Schlegel, K. (1996). A review of atmospheric gravity waves and travelling ionospheric disturbances: 1982-1995. *Annales Geophysicae, 14*, 917–940, https://doi.org/10.1007/s005850050357.

Huang, F., Dou, X., Lei, J., Lin, J., Ding, F., & Zhong, J. (2016). Statistical analysis of nighttime medium-scale traveling ionospheric disturbances using airglow images and GPS observations over central China. *Journal of Geophysical Research: Space Physics, 121*(9), 8887–8899. https://doi.org/10.1002/2016ja022760.

Huang, F., Lei, J., Dou, X., Luan, X., & Zhong, J. (2018). Nighttime Medium-Scale Traveling Ionospheric Disturbances from Airglow Imager and Global Navigation Satellite Systems Observations. *Geophysical Research Letters, 45*(1), 31–38. https://doi.org/10.1002/2017gl076408.

Huang, C.-S., Miller, C. A., & Kelley, M. C. (1994). Basic properties and gravity wave initiation of the midlatitude F region instability. *Radio Science, 29*(1), 395–405. https://doi.org/10.1029/93rs01669.

Hunsucker, R. D. (1982). Atmospheric gravity waves generated in the high-latitude ionosphere: A review. *Reviews of Geophysics, 20(2),* 293. https://doi.org/10.1029/rg020i002p00293.

Ichihara, A., Nishitani, N., Ogawa, T., Tsugawa, T. (2013). Northward propagating nighttime medium-scale traveling ionospheric disturbances observed with SuperDARN Hokkaido HF radar and GEONET. *Advances in Polar Science, 000(001),* 42–49. https://doi.org/10.3724/SP. J.1085.2013.00042.

Joshi, L. M., Sripathi, S., & Singh, R. (2016). Simulation of low-latitude ionospheric response to 2015 St. Patrick's Day super geomagnetic storm using ionosonde-derived PRE vertical drifts over Indian region. *Journal of Geophysical Research: Space Physics, 121(3),* 2489–2502. https://doi.org/10.1002/2015JA021512.

Kawamura, S., Otsuka, Y., Zhang, S.-R., Fukao, S., & Oliver, W. L. (2000). A climatology of middle and upper atmosphere radar observations of thermospheric winds. *Journal of Geophysical Research: Space Physics, 105(A6),* 12777–12788. https://doi.org/10.1029/2000ja900013.

Kelley, M. C., & Fukao, S. (1991). Turbulent upwelling of the mid-latitude ionosphere: 2. Theoretical framework. *Journal of Geophysical Research, 96(A3),* 3747. https://doi.org/10.1029/90ja02252.

Kelley, M. C., Makela, J. J., Swartz, W. E., Collins, S. C., Thonnard, S., Aponte, N., & Tepley, C. A. (2000). Caribbean Ionosphere Campaign, year one: Airglow and plasma observations during two intense mid-latitude spread-Fevents. *Geophysical Research Letters, 27(18),* 2825–2828. https://doi.org/10.1029/2000gl000022.

Kelley, M. C., & Makela, J. J. (2001). Resolution of the discrepancy between experiment and theory of midlatitude F-region structures. *Geophysical Research Letters, 28(13),* 2589–2592. https://doi.org/10.1029/2000GL012777.

Kelley, M. C., Makela, J. J., Paxton, L. J., Kamalabadi, F., Comberiate, J. M., & Kil, H. (2003). The first coordinated ground- and space-based optical observations of equatorial plasma bubbles. *Geophysical Research Letters, 30(14),* 1766. https://doi.org/10.1029/2003GL017301.

Mondal, S., Srivastava, A., Yadav, V., Sarkhel, S., Sunil Krishna, M. V., Rao, Y. K., & Singh, V. (2019). Allsky Airglow Imaging Observations from Hanle, Leh Ladakh, India: Image Analyses and First Results. *Advances in Space Research, 64*, 1926-1939. https://doi.org/10.1016/j.asr.2019.05.047.

Narayanan, V. L., Patra, A. K., Gurubaran, S., Pavan Chaitanya, P., & Emperumal, K. (2019). Coincident airglow, VHF radar, and ionosonde observations of electrified medium-scale traveling ionospheric disturbances in the equatorial latitudes. *Geophysical Research Letters, 46,* 7173–7181. https://doi.org/10.1029/2019GL083266.

Narayanan, V. L., Shiokawa, K., Otsuka, Y., & Saito, S. (2014). Airglow observations of nighttime medium-scale traveling ionospheric disturbances from Yonaguni: Statistical characteristics and low-latitude limit. *Journal of Geophysical Research: Space Physics, 119(11),* 9268–9282. https://doi.org/10.1002/2014ja020368.

Nicolls, M. J., Vadas, S. L., Aponte, N., and Sulzer, M. P. (2014). Horizontal parameters of daytime thermospheric gravity waves and E region neutral winds over Puerto Rico. *Journal of Geophysical Research: Space Physics, 119,* 575–600. https://doi.org/10.1002/2013JA018988.

Ogawa, T., Nishitani, N., Otsuka, Y., Shiokawa, K., Tsugawa, T., Hosokawa, K. (2009). Medium-scale traveling ionospheric disturbances observed with the SuperDARN Hokkaido radar, all-sky imager, and GPS network and their relation to concurrent sporadic E irregularities. *Journal of Geophysical Research: Space Physics, 114(A3),* n/a–n/a. https://doi.org/10.1029/2008JA013893.

Otsuka, Y., Onoma, F., Shiokawa, K., Ogawa, T., Yamamoto, M., & Fukao, S. (2007). Simultaneous observations of nighttime medium-scale traveling

ionospheric disturbances and E region field-aligned irregularities at midlatitude. *Journal of Geophysical Research: Space Physics, 112*(A6), n/a–n/a.). https://doi.org/10.1029/2005ja011548.

Otsuka, Y., Shiokawa, K., & Ogawa, T. (2004). Geomagnetic conjugate observations of medium-scale traveling ionospheric disturbances at midlatitude using all-sky airglow imagers. *Geophysical Research Letters, 31*(15). https://doi.org/10.1029/2004gl020262.

Otsuka, Y., Shiokawa, K., & Ogawa, T. (2012). Disappearance of equatorial plasma bubble after interaction with mid-latitude medium-scale traveling ionospheric disturbance. *Geophysical Research Letters, 39*(14). https://doi.org/10.1029/2012gl052286.

Otsuka, Y., Suzuki, K., Nakagawa, S., Nishioka, M., Shiokawa, K., & Tsugawa, T. (2013). GPS observations of medium-scale traveling ionospheric disturbances over Europe. *Annales Geophysicae, 31(2),* 163–172. https://doi.org/10.5194/angeo-31-163-2013.

Otsuka, Y., Tani, T., Tsugawa, T., Ogawa, T., & Saito, A. (2008). Statistical study of relationship between medium-scale traveling ionospheric disturbance and sporadic E layer activities in summer night over Japan. *Journal of Atmospheric and Solar-Terrestrial Physics, 70*(17), 2196–2202. https://doi.org/10.1016/j.jastp.2008.07.008.

Paulino, I., Medeiros, A. F., Vadas, S. L., Wrasse, C. M., Takahashi, H., Buriti, R. A., Leite, D., Filgueira, S., Bageston, J. V., Sobral, J. H. A., & Gobbi, D. (2016). Periodic waves in the lower thermosphere observed by OI630 nm airglow images. *Annales Geophysicae, 34*(2), 293–301. https://doi.org/10.5194/angeo-34-293-2016.

Paulino, I., Moraes, J. F., Maranhão, G. L., Wrasse, C. M., Buriti, R. A., Medeiros, A. F., Paulino, A. R., Takahashi, H., Makela, J. J., Meriwether, J. W., & Campos, J. A. V. (2018). Intrinsic parameters of periodic waves observed in the OI6300 airglow layer over the Brazilian equatorial region. *Annales Geophysicae, 36*(1), 265–273. https://doi.org/10.5194/angeo-36-265-2018.

Perkins, F. (1973). Spread F and ionospheric currents. *Journal of Geophysical Research, 78*(1), 218–226. https://doi.org/10.1029/ja078i001p00218.

Pimenta, A. A., Kelley, M. C., Sahai, Y., Bittencourt, J. A., & Fagundes, P. R. (2008). Thermospheric dark band structures observed in all-sky OI 630 nm emission images over the Brazilian low-latitude sector. *Journal of Geophysical Research: Space Physics, 113*(A1), n/a–n/a. https://doi.org/10.1029/2007ja012444.

Rathi, R., Yadav, V., Mondal, S., Sarkhel, S., Sunil Krishna, M. V., & Upadhayaya, A. K. (2021). Evidence for simultaneous occurrence of periodic and single dark band MSTIDs over geomagnetic low-mid latitude transition

region. *Journal of Atmospheric and Solar-Terrestrial Physics,* 215, 105588. https://doi.org/10.1016/j.jastp.2021.105588.

Rathi, R., Yadav, V., Mondal, S., Sarkhel, S., Sunil Krishna, M. V., Upadhayaya, A. K., Kannaujiya, S., Chauhan, P. (2022). A case study on the interaction between MSTIDs' fronts, their dissipation, and a curious case of MSTID's rotation over geomagnetic low-mid latitude transition region. *Journal of Geophysical Research: Space Physics, 127,* e2021JA029872. https://doi.org/10.1029/2021JA029872.

Rout, D., Chakrabarty, D., Sarkhel, S., Sekar, R., Fejer, B. G., Reeves, G. D., Kulkarni, A.S., Aponte, N., Sulzer, M., Mathews, J.D., Kerr, R.B., Noto, J. (2018), The ionospheric impact of an ICME-driven sheath region over Indian and American sectors in the absence of a typical geomagnetic storm. *Journal of Geophysical Research: Space Physics, 123(5), 4298–4308.* https://doi.org/10.1029/2018ja025334.

Rishbeth, H., Fuller-Rowell, T. J., & Rees, D. (1987). Diffusive equilibrium and vertical motion in the thermosphere during a severe magnetic storm: a computational study. *Planetary and Space Science, 35(9),* 1157–1165. https://doi.org/10.1016/0032-0633(87)90022-5.

Saito, S., Yamamoto, M., Hashiguchi, H., Maegawa, A., & Saito, A. (2007). Observational evidence of coupling between quasi-periodic echoes and medium scale traveling ionospheric disturbances. *Annales de Geophysique, 25(10),* 2185–2194. https://doi.org/10.5194/angeo-25- 2185-2007.

Sau, S., Lakshmi Narayanan, V., Gurubaran, S., & Emperumal, K. (2018). Study of wave signatures observed in thermospheric airglow imaging over the dip equatorial region. *Advances in Space Research.* https://doi.org/10.1016/j.asr.2018.06.039.

Shiokawa, K., Ihara, C., Otsuka, Y., & Ogawa, T. (2003a). Statistical study of nighttime medium-scale traveling ionospheric disturbances using midlatitude airglow images. *Journal of Geophysical Research, 108*(A1). https://doi.org/10.1029/2002ja009491.

Shiokawa, K., Otsuka, Y., Ihara, C., & Ogawa, T. (2003b). Ground and satellite observations of nighttime medium-scale traveling ionospheric disturbance at midlatitude. *Journal of Geophysical Research, 108*(A4). https://doi.org/10.1029/2002ja009639.

Shiokawa, K., Otsuka, Y., Tsugawa, T., Ogawa, T., Ohshima, K., Kubota, M., Maruyama, T., Nakamura, T., Yamamoto, M., & Wilkinson, P. (2005). Geomagnetic conjugate observation of nighttime medium-scale and large-scale traveling ionospheric disturbances: FRONT3 campaign. *Journal of Geophysical Research, 110*(A5). https://doi.org/10.1029/2004ja010845.

Shiokawa, K., Otsuka, Y., & Ogawa, T. (2006). Quasiperiodic southward moving waves in 630-nm airglow images in the equatorial thermosphere. *Journal of Geophysical Research, 111* (A6). https://doi.org/10.1029/2005ja011406.

Shiokawa, K., Mori, M., Otsuka, Y., Oyama, S., Nozawa, S., Suzuki, S., & Connors, M. (2013). Observation of nighttime medium-scale travelling ionospheric disturbances by two 630-nm airglow imagers near the auroral zone. *Journal of Atmospheric and Solar-Terrestrial Physics, 103*, 184-194. https://doi.org/10.1016/j.jastp.2013.03.024.

Shiokawa, K., Otsuka, Y., Lynn, K. J., Wilkinson, P., & Tsugawa, T. (2015). Airglow-imaging observation of plasma bubble disappearance at geomagnetically conjugate points. *Earth, Planets and Space, 67(1).* https://doi.org/10.1186/s40623-015-0202-6.

Sivakandan, M., Mondal, S., Sarkhel, S., Chakrabarty, D., Sunil Krishna, M. V., Chaitanya, P. P., et al. (2020). Mid-Latitude Spread-F Structures Over the Geomagnetic Low-Mid Latitude Transition Region: An Observational Evidence. *Journal of Geophysical Research: Space Physics*, *125*(5), 1–13. https://doi.org/10.1029/2019JA027531.

Sivakandan, M., Mondal, S., Sarkhel, S., Chakrabarty, D., Sunil Krishna, M. V., Upadhayaya, A. K., Shinbori, A., and Sori, T., Kannaujiya, S., Champati Ray, P. K. (2021). Evidence for the in-situ generation of plasma depletion structures over the transition region of geomagnetic low-mid latitude. *Journal of Geophysical Research: Space Physics, 126,* e2020JA028837. https://doi.org/10.1029/2020JA028837.

Sobral, J. H. A., Takahashi, H., Abdu, M. A., Muralikrishna, P., Sahai, Y., Zamlutti, C. J., … Batista, P. P. (1993). Determination of the quenching rate of the O(^{1}D) by O(^{3}P) from rocket-borne optical (630 nm) and electron density data. *Journal of Geophysical Research: Space Physics, 98(A5),* 7791–7798. https://doi.org/10.1029/92ja01839.

Sun, L., Xu, J., Wang, W., Yue, X., Yuan, W., Ning, B., Jhang, D., & de Meneses, F. C. (2015). Mesoscale field-aligned irregularity structures (FAIs) of airglow associated with medium-scale traveling ionospheric disturbances (MSTIDs). *Journal of Geophysical Research: Space Physics, 120*(11), 9839–9858. https://doi.org/10.1002/2014ja020944.

Sun, L., Xu, J., Xiong, C., Zhu, Y., Yuan, W., Hu, L., Liu, W., & Chen, G. (2019). Midlatitudinal special airglow structures generated by the interaction between propagating medium-scale traveling ionospheric disturbance and nighttime plasma density enhancement at magnetically quiet time. *Geophysical Research Letters.* https://doi.org/10.1029/2018gl080926.

Tsunoda, R. T., & Cosgrove, R. B. (2001). Coupled electrodynamics in the nighttime midlatitude ionosphere. *Geophysical Research Letters, 28(22),* 4171–4174. https://doi.org/10.1029/2001GL013245.

Upadhayaya, A. K., & Mahajan, K. K. (2013). IonosphericF2region: Variability and sudden stratospheric warmings. *Journal of Geophysical Research: Space Physics, 118(10),* 6736–6750. https://doi.org/10.1002/jgra.50570.

Vadas, S. L. (2007). Horizontal and vertical propagation and dissipation of gravity waves in the thermosphere from lower atmospheric and thermospheric sources. *Journal of Geophysical Research: Space Physics, 112(A6),* n/a–n/a. https://doi.org/10.1029/2006ja011845.

Vadas, S. L. and Fritts, D. C. (2005). Thermospheric responses to gravity waves: Influences of increasing viscosity and thermal diffusivity. *Journal of Geophysical Research, 110 (D15).* https://doi.org/10.1029/2004JD005574.

Yadav, V., Rathi, R., Gaur, G., Sarkhel, S., Chakrabarty, D., Sunil Krishna, M. V., Pavan Chaitanya, P., Patra, A. K., Choudhary, R. K., Pant, T. K., & Upadhayaya, A. K. (2021b). Interaction between mid-latitude field aligned plasma structure and medium scale traveling ionospheric disturbances during nighttime over geomagnetic low-mid latitude transition region. *Journal of Atmospheric and Solar-Terrestrial Physics,* 217, 105589. https://doi.org/10.1016/j.jastp.2021.105589.

Yadav, V., Rathi, R., Sarkhel, S., Chakrabarty, D., Sunil Krishna, M. V., & Upadhayaya, A. K. (2021a). A unique case of complex interaction between MSTIDs and mid-latitude field-aligned plasma depletions over geomagnetic low-mid latitude transition region. *Journal of Geophysical Research: Space Physics,* 126 (1), *e2020JA028620.* https://doi.org/10.1029/2020JA028620.

Yiğit, E., Medvedev, A. S., & Ern, M. (2020). Effects of latitude-dependent gravity wave source variations on the middle and upper atmosphere. *Frontiers in Astronomy and Space Sciences, 7.* https://doi.org/10.3389/fspas.2020.614018.

Yokoyama, T. (2013). Scale dependence and frontal formation of nighttime medium-scale traveling ionospheric disturbances. *Geophysical Research Letters, 40*(17), 4515–4519. https://doi.org/ 10.1002/grl.50905.

Yokoyama, T. (2014). Hemisphere-coupled modeling of nighttime medium-scale traveling ionospheric disturbances. *Advances in Space Research, 54,* 481–488. https://doi.org/10.1016/j.asr.2013.07.048.

Yokoyama, T., & Hysell, D. L. (2010). A new midlatitude ionosphere electrodynamics coupling model (MIECO): Latitudinal dependence and propagation of medium scale traveling ionospheric disturbances. *Geophysical Research Letters, 37*, L08105. https://doi.org/10.1029/2010GL042598.

Yokoyama, T., Hysell, D. L., Otsuka, Y., & Yamamoto, M. (2009). Three-dimensional simulation of the coupled Perkins and Es-layer instabilities in the nighttime midlatitude ionosphere. *Journal of Geophysical Research: Space Physics, 114(A3),* n/a–n/a. https://doi.org/10.1029/2008ja013789.

Zhou, Q., Mathews, J. D., Miller, C. A., & Seker, I. (2006). The evolution of nighttime mid-latitude mesoscale F-region structures: A case study utilizing numerical solution of the Perkins instability equations. *Planetary and Space Science, 54(7),* 710–718. https://doi.org/10.1016/j.pss.2006.03.005.

Figures

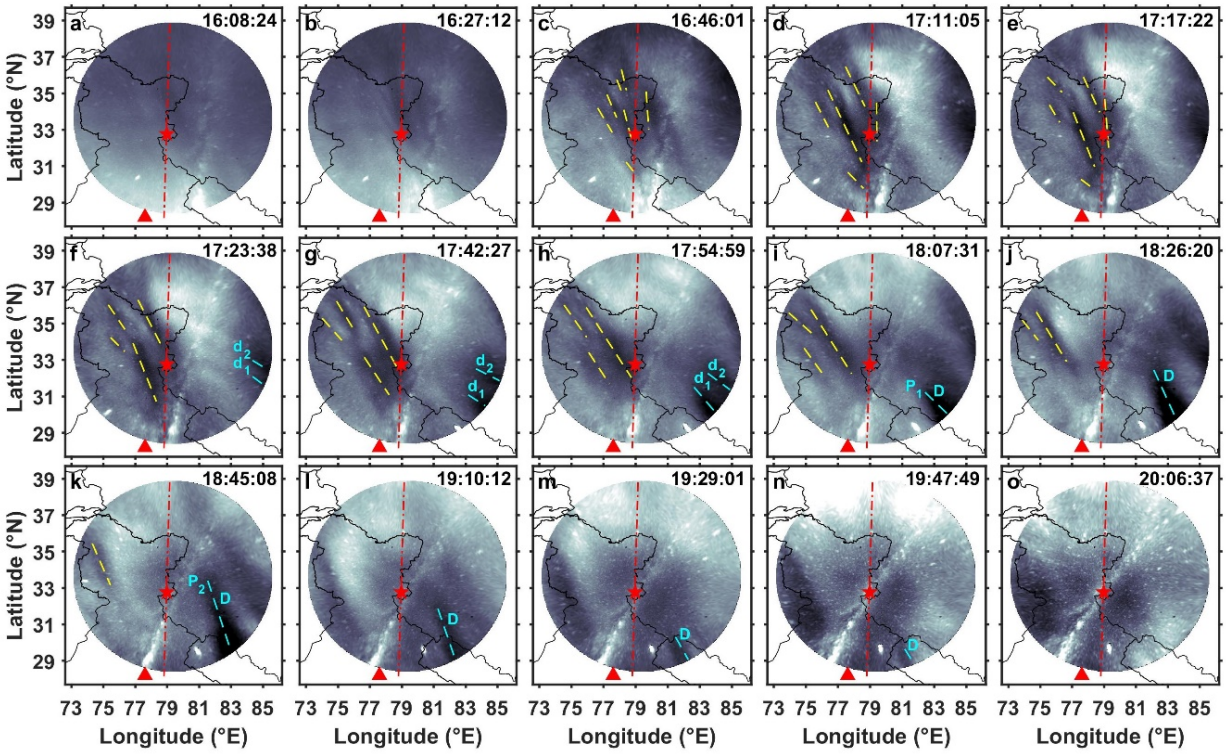

Figure 1: A time sequence of 630.0 nm airglow images showing three characteristically different structures on the quiet night of 08 July 2018. Red stars and triangles are indicating the positions of Hanle and New Delhi, respectively.

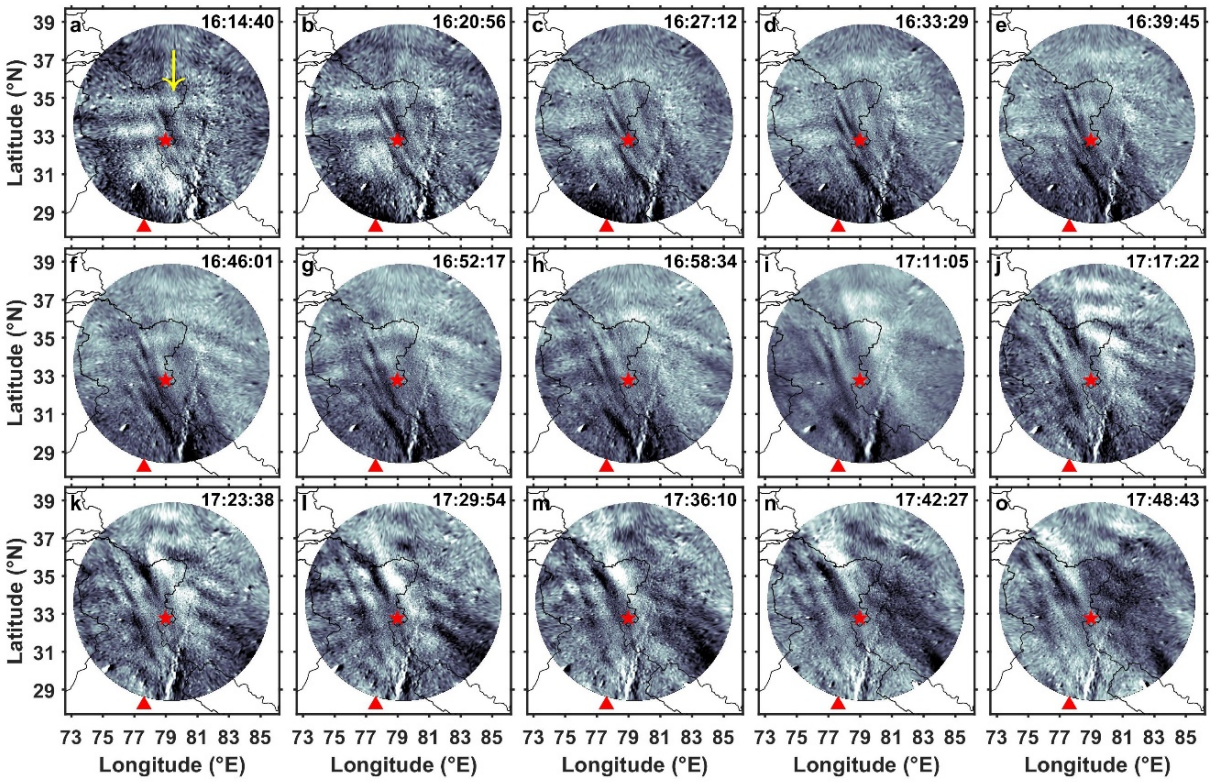

Figure 2: The successive difference images of 630.0 nm airglow images showing a wave-like structure propagating northward on the quiet night of 08 July 2018. Red stars and triangles are indicating the positions of Hanle and New Delhi, respectively.

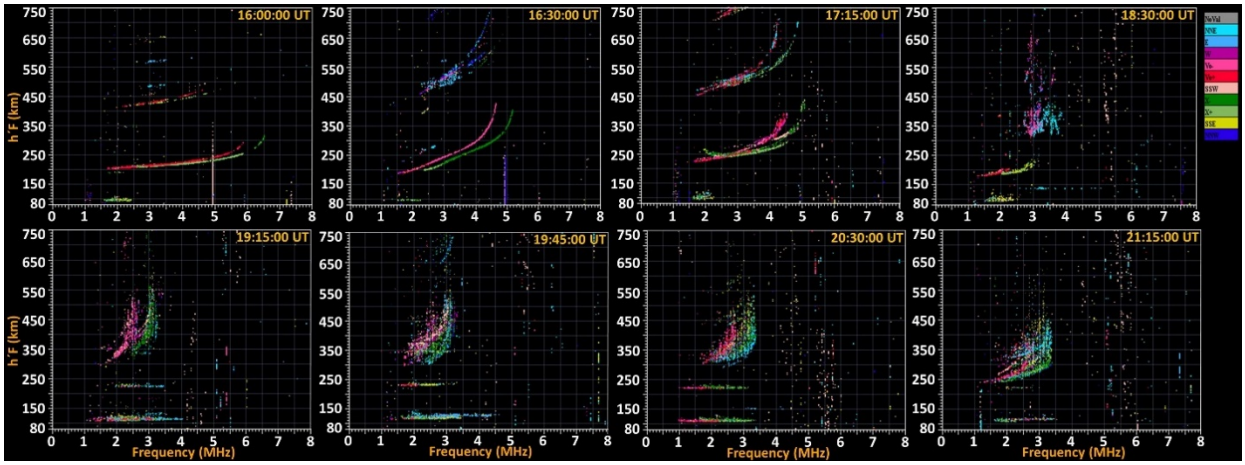

Figure 3: Ionogram sequence on the night of 08 July 2018, from New Delhi digisonde, showing rising and falling of F layer trace, and presence of spread F

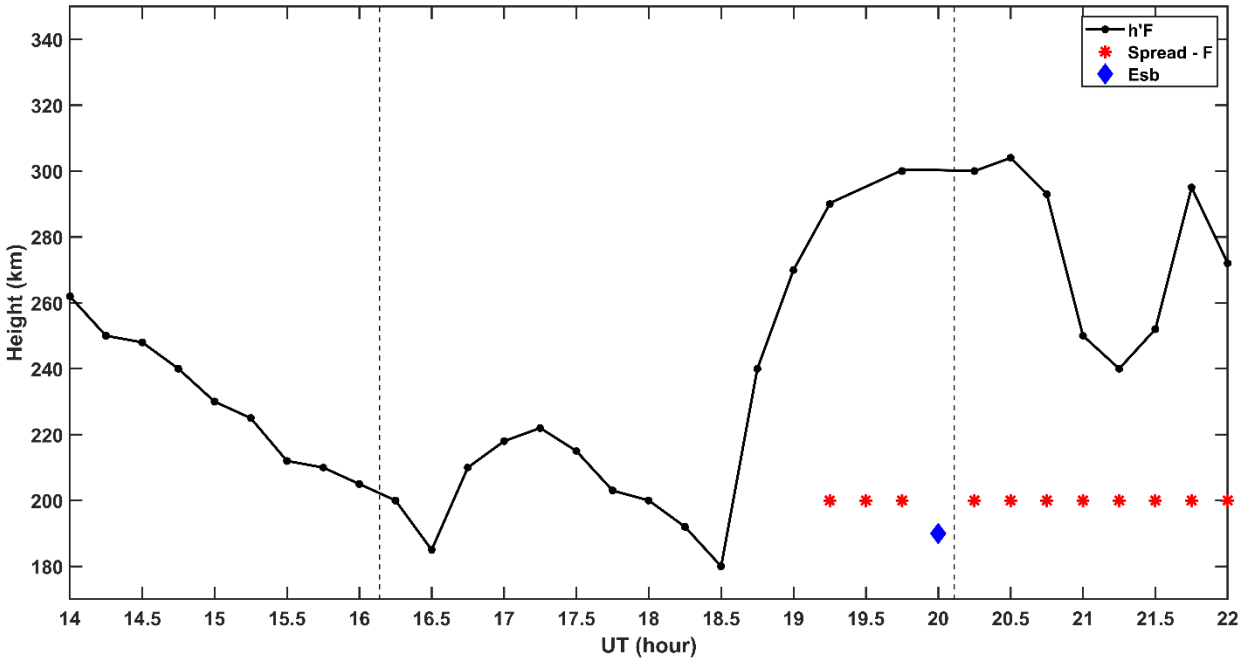

Fi

4: The variation of h'F over New Delhi. Red asterisks and blue diamond are showing the presence of spread F and blanketing sporadic E (Esb) layer, respectively.

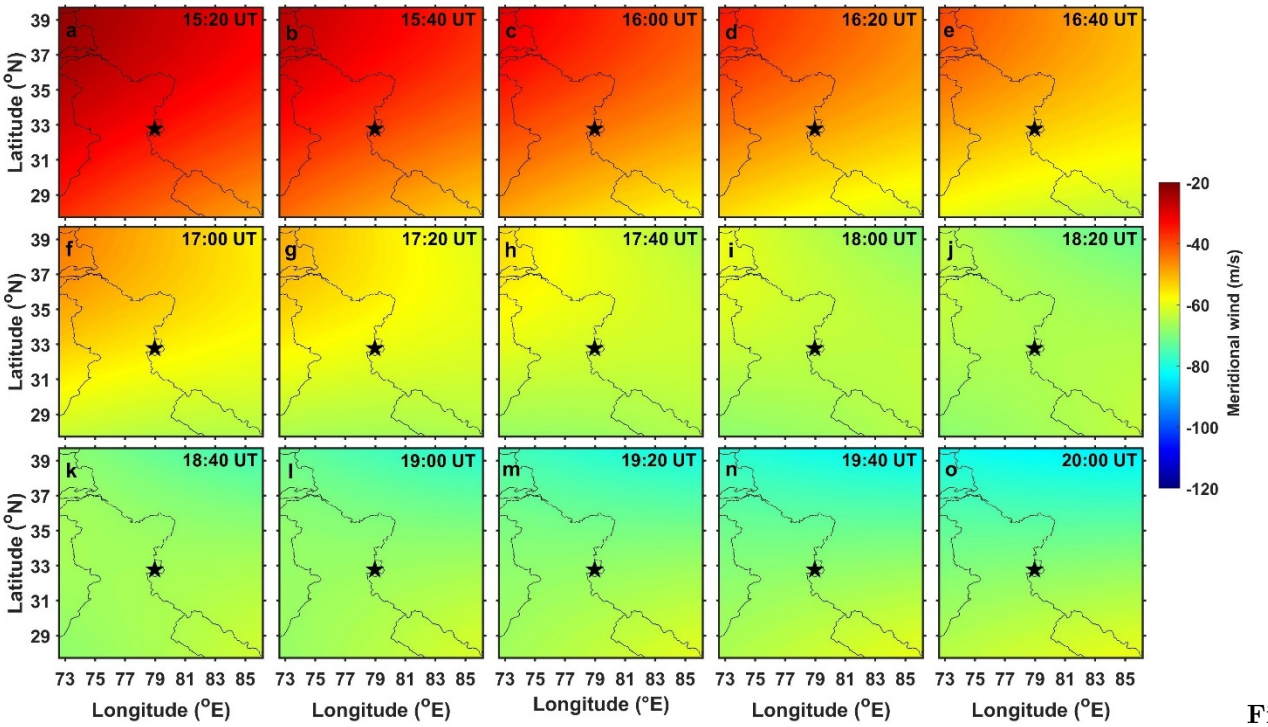

Fi

5: Time sequence of Meridional winds during the event. These values are derived by using HWM14 at an altitude of 250 km. Black star indicates the position of Hanle.

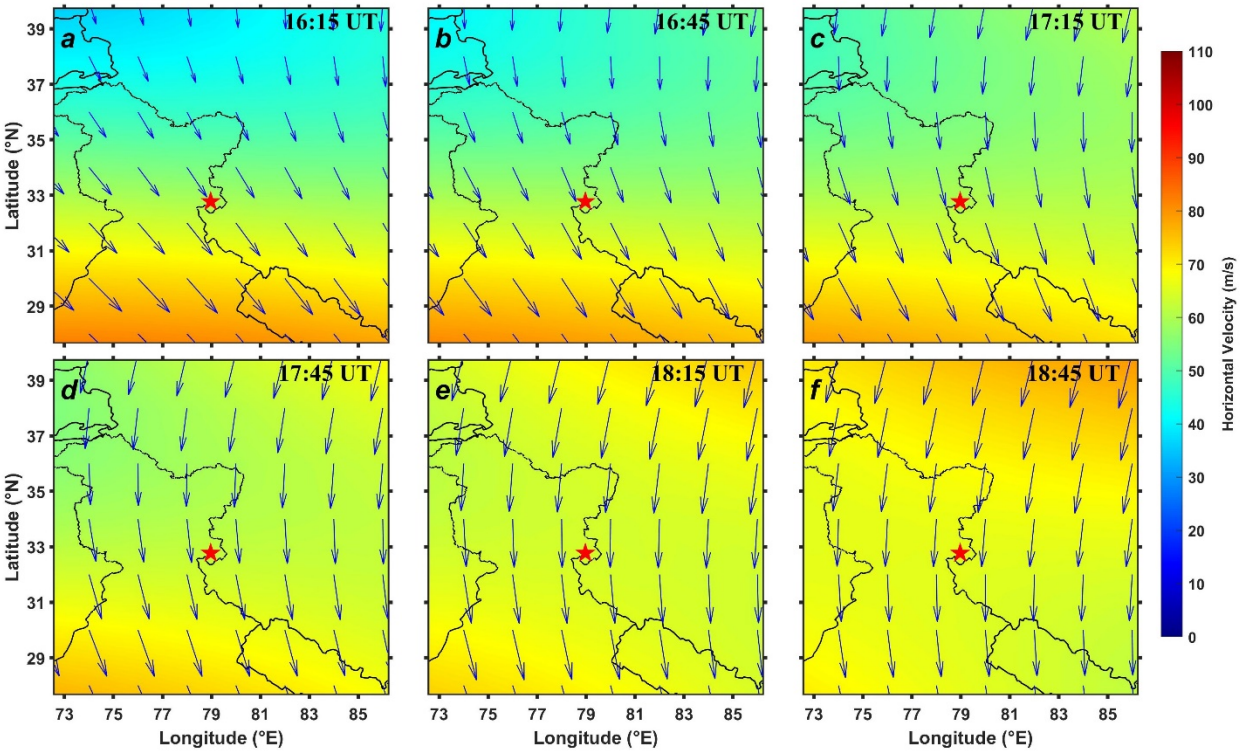

Figure 6: Time sequence of horizontal winds during the event. These values are derived by using HWM14 at an altitude of 250 km. Red star indicates the position of Hanle. Blue arrows represent the direction of the wind.